

A Microcanonical Inflection Point Analysis via Parametric Curves and its Relation to the Zeros of the Partition Function

J. C. S. Rocha,^{1,*} R. A. Dias,^{2,†} and B. V. Costa^{3,‡}

¹*Departamento de Física, ICEB, Universidade Federal de Ouro Preto - UFOP, Minas Gerais, Brasil.*

²*Departamento de Física, ICE, Universidade Federal de Juiz de Fora - UFJF, Minas Gerais, Brasil.*

³*Departamento de Física, ICEx, Universidade Federal de Minas Gerais - UFMG, Minas Gerais, Brasil.*

(Dated: February 4, 2025)

In statistical physics, phase transitions are arguably among the most extensively studied phenomena. In the computational approach to this field, the development of algorithms capable of estimating entropy across the entire energy spectrum in a single execution has highlighted the efficacy of microcanonical inflection point analysis, while Fisher's zeros technique has re-emerged as a powerful methodology for investigating these phenomena. This paper presents an alternative protocol for analyzing phase transitions based on parametric microcanonical curves. We also provide a clear demonstration of the relation of the linear pattern of the Fisher's zeros on the complex inverse temperature map (a circle in the complex $x = e^{-\beta\varepsilon}$ map) with the order of the transition, showing that the specific heat is inversely related to the distance between the zeros. We study various model systems, including the Lennard-Jones cluster, the Ising, the XY, and the Zeeman models, illustrating the characterization of first-order, second-order, and Berezinskii-Kosterlitz-Thouless (BKT) transitions, respectively. By examining the behavior of thermodynamic quantities such as entropy and its derivatives in the microcanonical ensemble, we identify key features—such as loops and discontinuities in parametric curves—which signal phase transitions' presence and nature. We are confident that this approach can facilitate the classification of phase transitions across various physical systems.

I. INTRODUCTION

Phase transitions are ubiquitous in nature, manifesting in phenomena such as the boiling of water and the demagnetization of a magnet. These transitions are among the best-understood emergent phenomena, where the collective behavior of the components results in substantial changes in the macroscopic properties of a system [1]. Understanding phase transitions is essential for fields like materials science, soft and condensed matter physics, and even cosmology [2–4]. The boiling of water, for instance, is characterized by the coexistence of liquid and vapor phases, with a clear distinction between the two states, whereas demagnetization shows no contrast between ferromagnetic and paramagnetic phases during the transition. According to P. Ehrenfest [5, 6], these phase transitions are classified as first-order and second-order, respectively. This classification is based on the lowest derivative of the free energy that is discontinuous or infinite at the transition point. In the early 1970s, a new type of phase transition was identified in two-dimensional systems, known as the Berezinskii-Kosterlitz-Thouless (BKT) transition. This transition, distinct from traditional phase transitions, is driven by the behavior of topological defects and has been observed in specific magnetic systems, in superconducting and superfluid films [7]. In this work, we employ the framework of statistical physics

to contribute to the development of an analytical scheme for studying these phenomena.

From the statistical physics perspective, the thermodynamics of an isolated system is described by the microcanonical ensemble. The fundamental equation in this ensemble is the entropy, given by

$$S(E) = k_B \ln \Omega(E), \quad (1)$$

where $\Omega(E)$ represents the number of states with energy E , and k_B denotes the Boltzmann constant [8]. This expression encapsulates all the essential information required to describe the system. Following the axiomatic approach of Callen [9], entropy is a strictly monotonically increasing and concave function. The presence of a convex region in the entropy function indicates thermodynamic instability. Specifically, a change in the curvature of $S(E)$ signals a first-order phase transition [10, 11].

Canonically, a phase transition is indicated by large fluctuations in some physical quantity as the average energy, as evidenced by singularities in the specific heat. In contrast, since the temperature remains constant throughout the phase transition, it is expected that the inverse microcanonical temperature,

$$\bar{\beta}(E) = \frac{1}{\bar{T}} = \left(\frac{\partial S}{\partial E} \right)_{\{X\}}, \quad (2)$$

minimally respond to changes in energy. Therefore, a first-order phase transition is identified by a local minima on $\bar{\beta}(E)$. The overbar denotes that we are specifically referring to microcanonical temperatures. It is important to note that, in the thermodynamic limit, \bar{T} converges to the regular temperature, T , usually associated with a

* jcsrocha@ufop.edu.br

† rodrigo.dias@ufjf.br

‡ Retired Professor; bvc@fisica.ufmg.br

heat bath. Moreover, $\{X\} = V, N, M, \dots$ represents a set of independent extensive parameters such as volume, V , number of particles, N , magnetization, M , and so forth, that characterize the thermodynamic system.

Furthermore, the occurrence of a convex intruder in the entropy during a first-order transition results in multiple energy values sharing the same $\bar{\beta}$. By solving eq. (2) for E , i.e. $E = E(\bar{\beta})$, and inserting it into eq. (1), one obtains an expression for the entropy in terms of the inverse temperature, $S = S(\bar{\beta})$. This implies that the microcanonical parameters can be expressed as parametric equations. However, this is not a one-to-one transformation, due to the shared β values among multiple energies, these parameterized microcanonical quantities fail to satisfy the condition of domain uniqueness of a function in the unstable region. This feature can be used as a criterion for identifying phase transitions¹.

In the case of a system in thermal contact with a heat bath, its statistical description is given by the canonical ensemble. The partition function, Z , is the fundamental quantity in this context. Mathematically, this function can be interpreted as the Laplace transform of $\Omega(E)$, i.e.

$$Z(\mathcal{B}) = \int \Omega(E) e^{-\mathcal{B}E} dE, \quad (3)$$

where $\mathcal{B} = \beta + i\tau$ represents a complex inverse temperature, with $\beta = 1/k_B T$ denoting the regular canonical inverse temperature [12, 13]. The canonical ensemble is connected to thermodynamics through the Helmholtz free energy, given by

$$F(\mathcal{B}) = -\frac{1}{\mathcal{B}} \ln Z(\mathcal{B}). \quad (4)$$

Although the complex temperature lacks physical meaning, the analytic continuation of the free energy can reveal phase transitions at the limit of $\tau \rightarrow 0$ [14]. Specifically, in the Fisher's zeros analysis [15], phase transitions are identified by the points where

$$\lim_{\substack{N \rightarrow \infty \\ \tau \rightarrow 0}} Z(\mathcal{B}) \rightarrow 0. \quad (5)$$

Examination of equations (4) and (5) reveals that the zeros of the partition function correspond to the nonanalytic points of the free energy, which manifest as discontinuities and singularities characteristic of phase transitions.

The main goal of this manuscript is to propose a modified microcanonical inflection point analysis that incorporates parametric curves. Additionally, we aim to demonstrate the relationship between Fisher's zeros maps and these curves. The proposed study is applied to well-known models with first and second-order transitions, as well as to models presenting BKT transition and no

transitions as a matter of comparison. The motivation for studying various types of transition extends beyond illustrating the proposed analysis; it also has the potential to be used in the development of classifiers within an Artificial Intelligence framework designed to categorize phase transitions[16].

This paper is structured as follows. In subsection II A, we present the fundamental concepts of the Fisher Zeros analysis. Following that, in subsection II A 1, we provide an alternative and simplified demonstration of the connection between the pattern of zeros maps and the unstable region of the entropy, as previously reported [17]. In the demonstration provided here, we show that the latent heat can be determined by the distance between the zeros in the pattern associated with the first-order transition. In subsection II B, we discuss the microcanonical inflection point analysis and introduce its parametric formulation. Section III presents results for various models: the Lennard-Jones cluster in subsection III A as a prototype of a first-order transition, the Ising model in subsection III B as an example of a second-order transition, the XY model in subsection III C to study the BKT transition, and the Zeeman model in subsection III D as a case with no transition. Section IV outlines our conclusions and offers perspectives for future work.

II. METHODOLOGY

A. Fisher's Zeros

By introducing a discretization with an energy gap ε , such that the energy of the k^{th} level can be expressed as $E_k = E_0 + k\varepsilon$, where E_0 denotes the ground state energy and $k = 0, 1, 2, \dots$, the partition function, eq. (3), takes the form

$$Z_N(\mathcal{B}) = e^{-\mathcal{B}E_0} \sum_{k=0}^{\Gamma} \Omega_k e^{-\mathcal{B}k\varepsilon}, \quad (6)$$

where $\Omega_k \equiv \Omega(E_k)$ and Γ is the number of energy levels. Following Fisher, we define a new variable:

$$x := e^{-\varepsilon\mathcal{B}} = e^{-\varepsilon\beta} e^{-i\varepsilon\tau}, \quad (7)$$

so that the partition function is now written as a polynomial:

$$Z = e^{-\mathcal{B}E_0} \sum_{k=0}^{\Gamma} \Omega_k x^k = e^{-\mathcal{B}E_0} \prod_{k=1}^{\Gamma} (x - x_k). \quad (8)$$

Where x_k are the zeros of the polynomial. It is worth mentioning that these roots occur in complex conjugate pairs, i.e; $x_{k\pm} = e^{-\varepsilon\beta_k} e^{\pm i\varepsilon\tau_k}$.

Since the polynomial's coefficients $\Omega_k \geq 0$, $\forall k$, any real zeros must be negative. However, it is well-known that phase transitions are defined in the thermodynamic limit. Hence, it is expected that a particular zero, or a

¹ See Chapter 9 in ref. [9], more specifically Sections 9-4 and 9-5

set of zeros, will consistently approach the real positive axis as the system size increases. Those zeros are called dominant or leading zeros, and they pinch the positive real axis in the thermodynamic limit. With this fact in mind, a finite-size scaling (FSS) analysis can be employed to detect the phase transition points. The dominant zeros exhibit a power law behavior with the system size L as:

$$x_k \propto L^{-\nu}, \quad (9)$$

where ν is the critical exponent of the correlation length [18]. Therefore, the analysis of the Fisher zeros consists of studying how the partition function approaches zero, i.e. $\lim_{L \rightarrow \infty} Z(\mathcal{B}_k, L) \rightarrow 0$.

1. Zeros Map Pattern for the First-Order Transition

Recently we have shown the connection of the unstable region of the entropy to the pattern of the Fisher zeros map [17]. Specifically, this region leads to a vertical line in a complex inverse temperature map. This line corresponds to a circle in the x -map (see eq. (7) for the definition of x). Here we present a simpler version of the demonstration presented in Ref. [17].

The demonstration here is based on the well-established double-tangent line construction across the convex region of the entropy. This construction was proposed to force $S(E)$ to obey the stability condition by eliminating the convex intruder². The slope of this line, $\bar{\beta}_{tan}$, can also be recognized as an estimate of the inverse transition temperature. The points of tangency define the energy range of the transition $[E', E'']$. Since heat is given by $dQ = TdS$, the latent heat can be given by

$$\mathcal{L} = \bar{T}_{tan} \Delta S, \quad (10)$$

where $\bar{T}_{tan} = 1/\bar{\beta}_{tan}$ and $\Delta S = S(E'') - S(E')$.

Inspired by the work of Taylor et al. [20], which calculated the zeros map just in the unstable region of the entropy, we claim that

$$Z'(\mathcal{B}_j) = \sum_{E=E'}^{E''} \Omega(E) e^{-\mathcal{B}_j E} \approx 0. \quad (11)$$

This approach can be justified by the Fisher's zeros analysis that truncates the energy range [21–24].

Let us consider the linear equation that describes the double-tangent line as

$$S^*(E) \approx S_0^* + \bar{\beta}_{tan} E, \quad (12)$$

where S_0^* is the value where the line intercepts the ordinate axis. The asterisk indicates that this approach for

the entropy is valid just in unstable regions. In the energy range considered, $E = E' + \ell\varepsilon$, where $\ell = 0, 1, \dots, n'$ and $n' = (E'' - E')/\varepsilon$. Then

$$S^*(E) \approx S' + \bar{\beta}_{tan} \varepsilon \ell, \quad (13)$$

where $S' = S_0^* + \bar{\beta}_{tan} E'$ is a rescaled constant. By inserting eq. (13) into eq. (1), solving it for Ω , then defining

$$x := e^{-\varepsilon(\mathcal{B} - \frac{\bar{\beta}_{tan}}{k_B})} = e^{-\varepsilon(\beta - \frac{\bar{\beta}_{tan}}{k_B})} e^{-i\varepsilon\tau}, \quad (14)$$

we can rewrite eq. (11) as

$$Z' \approx e^{-\mathcal{B}F'} \sum_{\ell=0}^{n'} x^\ell = e^{-\mathcal{B}F'} \frac{1 - x^{n'+1}}{1 - x}, \quad (15)$$

where $F' = E' - S'/(k_B \mathcal{B})$. By inspecting eqs. (15) and (14), we get $Z' = 0$ if

$$\beta_j = \frac{\bar{\beta}_{tan}}{k_B}, \quad (16)$$

and

$$\tau_j = \frac{2\pi}{\varepsilon(n'+1)} j \approx \frac{2\pi}{\mathcal{L}} j, \quad (17)$$

where \mathcal{L} is given by eq. (10) and $j = 1, 2, \dots, n'$. The approach in the last term is valid for $n' \gg 1$ ($\varepsilon n' = E'' - E' = \Delta E$ and $\bar{T}_{tan} = \Delta E/\Delta S$). It is worth mentioning that $j \neq 0$ and $j \neq (n'+1)$, since the denominator in the last term of eq. (15) requires that $x \neq 1$, hence \mathcal{B}_j can not be a positive real number, as expected for finite systems. Furthermore, any other j will lead to multiplicities and can be neglected. Since $\bar{\beta}_{tan}$ is a constant, plotting the ordered pairs (β_j, τ_j) leads to a vertical line of evenly spaced points, as claimed before. Moreover, the distance between these zeros is inversely proportional to the latent heat. A graphical representation of these descriptions is presented in Section III A 2.

B. Microcanonical Analysis

The state of an isolated thermodynamic system in equilibrium is characterized by the derivatives of the entropy, eq (1). As mentioned, the inverse microcanonical temperature is defined as

$$\bar{\beta}(\mathbf{e}) = \left(\frac{\partial s}{\partial \mathbf{e}} \right)_{\{X\}}, \quad (18)$$

where $\mathbf{s} = S/N$, $\mathbf{e} = E/N$ are the entropy and the energy densities, respectively. It is worth emphasizing that we reserve the italic letter, e , to the Euler's number.

Furthermore, the stability condition which requires that $\mathbf{s}(\mathbf{e})$ be a monotonically increasing concave function,

² For more details, see Chapter 8 in ref [9] and Section 2.7 in Ref. [19].

ensures that $\bar{\beta}$ is a monotonically decreasing convex positive function. Higher-order derivatives of entropy,

$$\gamma(\mathbf{e}) = \left(\frac{\partial^2 \mathbf{s}}{\partial \mathbf{e}^2} \right)_{\{X\}} \quad \text{and} \quad \delta(\mathbf{e}) = \left(\frac{\partial^3 \mathbf{s}}{\partial \mathbf{e}^3} \right)_{\{X\}}, \quad (19)$$

are, respectively, an increasing concave negative function, and a decreasing convex positive function, and so on. In this work, entropy is a function of a single variable, i.e. $\mathbf{s} = \mathbf{s}(\mathbf{e})$, the partial derivative is effectively equivalent to the total derivative and can be used interchangeably in this context.

1. The microcanonical inflection point analysis

Based on the principle of minimal sensitivity [25, 26], a new method was recently proposed to characterize phase transitions by identifying least-sensitive inflection points (LSIPs) in the entropy and its derivatives [27]. According to this approach, in general, an independent phase transition of odd order $(2k - 1)$ can be identified if there is an LSIP in the $(2k - 2)$ -th derivative of the entropy and a corresponding minimum in the $(2k - 1)$ -th derivative, i.e.,

$$\left. \frac{d^{2k-1} \mathbf{s}}{d\mathbf{e}^{2k-1}} \right|_{\mathbf{e}=\mathbf{e}_{tr}} < 0 \quad (20)$$

where $k = 1, 2, \dots$, and \mathbf{e}_{tr} represents the energy at the LSIP. Notably, as mentioned in the introduction, for a first-order transition, an LSIP in the entropy results in a local minimum at $\mathbf{e} = \mathbf{e}_{tr}$ in the inverse temperature. This minimum point defines the transition temperature $\bar{T}_{tr} = 1/\bar{\beta}_{tr}$, where $\bar{\beta}_{tr} = \bar{\beta}(\mathbf{e}_{tr})$.

Likewise, an independent phase transition of even order $2k$ occurs if there is a least-sensitive inflection point in the $(2k - 1)$ -th derivative of the entropy and a corresponding negative-valued maximum in the $(2k)$ -th derivative, i.e.,

$$\left. \frac{d^{2k} \mathbf{s}}{d\mathbf{e}^{2k}} \right|_{\mathbf{e}=\mathbf{e}_{tr}} > 0. \quad (21)$$

Additionally, another type of transition, which occurs concomitantly with an independent transition of a lower order, can be identified. A dependent transition of even order $2k$ is signaled by the presence of an LSIP in the $(2k - 1)$ -th derivative of the entropy. This can be recognized by a positive-valued minimum in the $(2k)$ -th derivative within the transition region of the corresponding independent transition, i.e.,

$$\left. \frac{d^{2k} \mathbf{s}}{d\mathbf{e}^{2k}} \right|_{\mathbf{e}=\mathbf{e}_{tr}} > 0. \quad (22)$$

And a dependent transition of odd order $(2k + 1)$ is indicated by the presence of an LSIP in the $2k$ -th derivative

of the entropy and is determined by a negative-valued maximum in the $(2k + 1)$ -th derivative, i.e.,

$$\left. \frac{d^{2k+1} \mathbf{s}}{d\mathbf{e}^{2k+1}} \right|_{\mathbf{e}=\mathbf{e}_{tr}} < 0 \quad (23)$$

It is worth mentioning that the existence of an independent transition is a necessary condition for a dependent transition, but the former can occur without the presence of the latter.

Specifically, for the independent second-order phase transition, \mathbf{e}_{tr} is defined at the negative-valued peak of γ . The corresponding critical temperature is then $T_C = 1/\bar{\beta}_{tr}$. Beyond that,

$$\lim_{N \rightarrow \infty} \gamma_{tr} \rightarrow 0, \quad (24)$$

where $\gamma_{tr} = \gamma(\mathbf{e}_{tr})$. In earlier studies, a positive-valued peak of γ was also used to define a first-order phase transition [19, 28]. Similarly, the limit presented in eq. (24) is equally valid for the earlier studies.

2. The parametric microcanonical inflection point analysis

A direct analogy can be drawn between Fisher zero analysis and microcanonical methods, as mathematically evident from eqs. (5) and (24), both approaches involve investigating the behavior of a specific function as it approaches zero. Recognizing that $Z = Z(\beta)$ and $\gamma = \gamma(\mathbf{e})$, i.e., they are functions of distinct variables, we propose examining both within the framework of a unified parameter.

As alluded in the introduction, eq. (18) can be solved for \mathbf{e} , yielding $\mathbf{e} = \mathbf{e}(\bar{\beta})$, which allows for the derivation of parametric curves such as $\mathbf{s} = \mathbf{s}(\bar{\beta})$, $\gamma = \gamma(\bar{\beta})$ and so forth. These parametric representations, as discussed, fail to satisfy the condition of domain uniqueness of a function in the unstable region. Moreover, as $\bar{\beta}$ remains bounded at the transition point, eq. (24) continues to be valid for the parametric representation.

In this study, we propose defining a first-order transition in regions where the microcanonical parametric curves fail to exhibit the properties of a function. Specifically, for a first-order phase transition, the parametric curve for the entropy forms a Z-like path. This behavior allows for an equal-area Maxwell construction to enforce $\mathbf{s}(\bar{\beta})$ being a function. Additionally, acting in accordance with earlier microcanonical analysis studies, the analysis of γ indicates a loop in the parametric curve, with the knot point serving as the indicator of the transition temperature. This loop structure effectively captures the behavior associated with the transition, complementing the insights gained from the parametric curve analysis of entropy. In contrast, for second-order phase transitions, the analysis of the parametric curve is consistent with conventional microcanonical analysis, characterized by a negative-valued peak in $\gamma(\bar{\beta})$. The BKT transition is the

most well-known example of an infinite-order phase transition. Given the mathematical intractability of evaluating infinite derivatives, the microcanonical analysis initially appears unfeasible in this context. Nevertheless, we explored whether discernible signatures of this transition could be observed in lower-order derivatives. The following section provides graphical illustrations of all these transitions within the present framework.

III. RESULTS

A. Lennard-Jones Cluster

We consider N particles interacting via the Lennard-Jones (LJ) potential as a case study of the first-order phase transitions. The LJ potential can be written as:

$$U_{LJ}(r_{ij}) = 4\epsilon \left[\left(\frac{\sigma}{r_{ij}} \right)^{12} - \left(\frac{\sigma}{r_{ij}} \right)^6 \right], \quad (25)$$

where $r_{ij} = |\mathbf{r}_j - \mathbf{r}_i|$ is the distance between the particles i and j . We chose a reduced unit system such that $\epsilon = 1$ and $\sigma = 2^{-1/6}$, the latter was chosen to lead the minimum of the potential at distance $r_{ij} = r_0 = 1$.

Recently, we conducted an extensive study of this model using the traditional microcanonical inflection point and the Fisher's zeros map analysis [17], both derived from DOS obtained via the Replica Exchange Wang-Landau (REWL) method [29–31]. In this previous study, we considered $N = 147$ particles confined to a sphere of radius $r_c = 4\sigma$ to reproduce the transition temperature ($T \approx 0.36$) reported in the literature [32]. We determined the transition temperatures to be $\bar{T}_{tr} = 0.3666(8)$ from the microcanonical inflection point, $\bar{T}_{tan} = 0.364(1)$ from the double tangent line construction, and $T_1/k_B = 0.3622(3)$ from the leading zeros of the Fisher's zeros map. Additionally, we demonstrated the linear behavior of the dominant zeros. It is worth mentioning that, for finite systems, different quantities provide distinct transition temperatures, which converge to a single transition value as the thermodynamic limit is approached [33]. In order to authenticate the parametric approach to the microcanonical analysis, we will reuse the same set of raw data in this present study, shown in the following Section.

To illustrate the scaling behavior of γ described by eq. (24), we simulate $N = 55$ particles inside a sphere of radius $r_c = 3.5\sigma$, also chosen to reproduce the transition temperature ($T \approx 0.29$) reported in the literature [32]. Besides that, it is claimed that the results for the LJ-cluster are independent of the volume if it does not compress the intact cluster [34]. This condition can be obeyed by considering densities (N/V) lower than that of the bulk liquid at the triple point. For the case of 147 particles, it means $r_c > 3.7\sigma$ and for 55 particles $r_c > 2.6\sigma$ [34]. Therefore, to gain insight into the behavior of the Fisher's zeros pattern along the first-order

transition line, we also study a system of $N = 147$ particles confined within a sphere of radius $r_c = 3.5\sigma$. Both considerations are presented in Section III A 2.

1. The parametric microcanonical inflection point analysis for $N = 147$ particles inside a sphere of radius $r_c = 4.0\sigma$

To illustrate the proposal analysis, Fig. 1 depicts in the solid black line the entropy per spin as a function of the energy density, $s(\mathbf{e})$, for the 147 particles inside a sphere of radius $r_c = 4.0\sigma$. It is worth emphasizing that $s(\mathbf{e})$ is the output of the REWL simulations, moreover, in this work error bars equal or smaller than the symbol are not shown. The double tangent line construction is shown by the dotted black line. The red dashed curve in this graph represents the microcanonical inverse temperature, $\bar{\beta}(\mathbf{e})$, obtained by the derivative of the black line, as given by eq. (18). For each value of \mathbf{e} , we plot the ordered triple $(\mathbf{e}, \bar{\beta}, s)$, illustrated by black circles. The projection of this curve onto the $s \times \bar{\beta}$ -plane yields the parametric curve $s(\bar{\beta})$, shown as the dotted-dashed blue curve³. This curve is detailed in Fig. 2, where the temperature obtained from the Fisher's zeros analysis leads to the hued regions $A_1 \approx A_2$. Therefore, the temperature of the leading zero corroborates with equal area construction, which is proposed to adjust $s(\bar{\beta})$ to comply with the uniqueness domain criteria of a function by eliminating the original points in the shaded regions and replace them by the vertical line. Consequently, this construction leads to the discontinuity of entropy, a defining feature in the modern classification of phase transitions. A visual inspection in Fig. 1 demonstrates that the equal area construction on $s(\bar{\beta})$ is clearer than the double tangent line construction on the convex intruder on $s(\mathbf{e})$. This clarity facilitates the estimation of latent heat and aids in determining the order of the transition. Moreover, in the Fig. 2, we measured the latent heat to be $\mathcal{L} = 55.1(3)$. Inserting this value into eq. (17), it leads to $\Delta\tau = \tau_{j+1} - \tau_j = 0.1150(8)$, which differ by only 4.5% from the average of the distances between the dominant zeros, $\langle \Delta\tau \rangle = 0.110(2)$, measured on the zeros maps [17]. This result further supports the proposed approach.

Fig. 3 demonstrates a similar process for obtaining the parametric curve $\gamma(\bar{\beta})$, which is shown in detail in

³ The projection of the triple $(\mathbf{e}, \bar{\beta}, s)$ onto the $s \times \bar{\beta}$ -plane is a graphical construction. We save our data into a file where the first column represents the energy density (\mathbf{e}), the second column represents the entropy (s), and the subsequent columns represent the first ($\bar{\beta}$), second (γ), and third (δ) derivatives of s with respect to \mathbf{e} . Instead of plotting s against \mathbf{e} we plot s against $\bar{\beta}$, where s and $\bar{\beta}$ correspond to the same \mathbf{e} . This procedure is similarly applied to the other quantities. Moreover, the curve $s(\mathbf{e})$ obtained from the REWL was fitted using a Bézier curve, and the derivatives of s were taken as the derivatives of the Bézier curve, which are also Bézier curves, see section 4.3 in the book cited in Ref. [19].

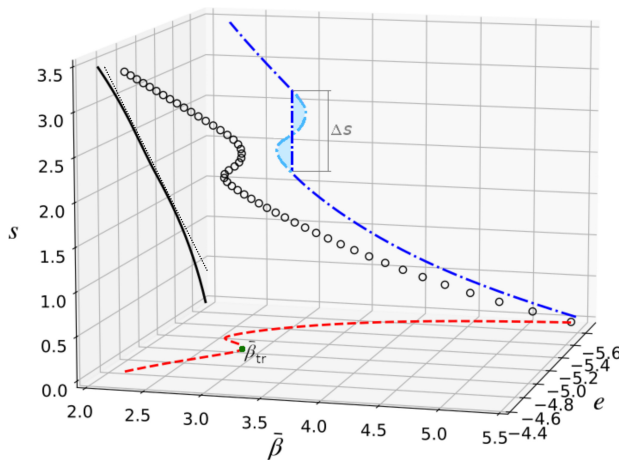


FIG. 1. (Color online) The entropy per spin, considered as a function of energy density and inverse temperature, $s(\mathbf{e}, \bar{\beta})$, for the 147-LJ cluster inside a sphere of radius $r_c = 4.0\sigma$.

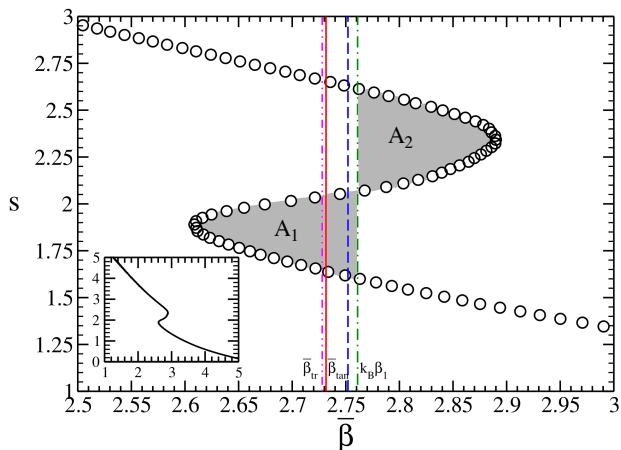


FIG. 2. (Color online) Parametric curve defined by the entropy per particles, $s(\mathbf{e})$, and the microcanonical inverse temperature, $\bar{\beta}(\mathbf{e})$, for the 147-LJ cluster. The inset provides a broader view of the curve. The hued regions $A_1 \approx A_2$ represent the equal areas construction.

Fig. 4. Additionally, Fig. 3 illustrates the regular microcanonical inflection point analysis by the dotted black line. This line projects the energy of the peak position of $\gamma(\mathbf{e})$ onto $\bar{\beta}(\mathbf{e})$, leading to $\bar{\beta}_{tr} = \bar{\beta}(\mathbf{e}_{tr})$. The loop on the parametric curve $\gamma(\bar{\beta})$ for the first-order transition is illustrated in this figure. By applying the uniqueness domain criterion for functions, the curve is truncated at the knot position, thereby eliminating the loop points and defining the transition temperature at this position. In Fig. 4 we measured the temperature of the knot position to be $\bar{T}_{knot} = 0.3660(1)$. It is worth mentioning that $|\bar{T}_{tr} - \bar{T}_{knot}|$ is smaller than the error of \bar{T}_{tr} , where \bar{T}_{tr} is the transition temperature obtained from the regular microcanonical analysis. Additionally, the latent heat was calculated using all estimated transition temperatures, with the results differing within the er-

ror bars. Specifically, in addition to the previously mentioned $\mathcal{L}_1 = 55.1(3)$ obtained from β_1 , we find that β_{tr} yields $\mathcal{L}_{tr} = 55.0(6)$, β_{tan} estimates $\mathcal{L}_{tan} = 54.2(7)$, and β_{knot} measures $\mathcal{L}_{knot} = 54.7(2)$. This yields an average value of $\mathcal{L}_{avg} = 54.8(5)$.

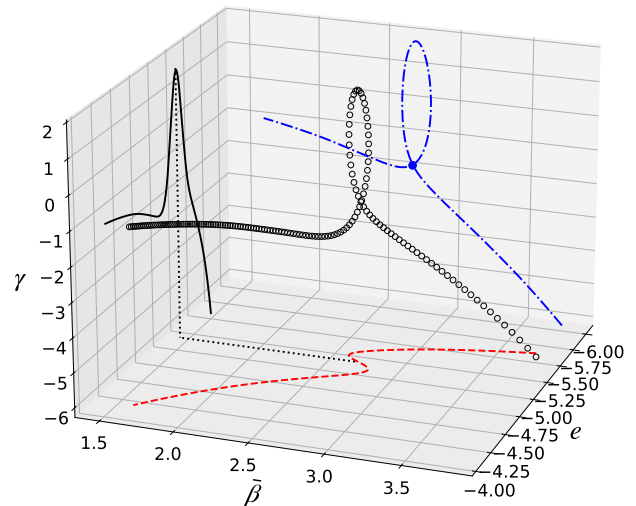


FIG. 3. (Color online) The second derivative of the entropy with respect to the energy density, considered as a function of energy density and inverse temperature, $\gamma(\mathbf{e}, \bar{\beta})$, for the 147-LJ cluster.

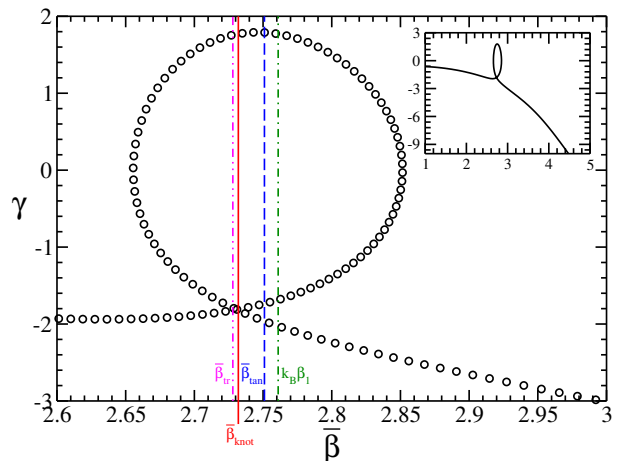


FIG. 4. (Color online) Parametric curve defined by the second derivative of the entropy with respect to energy, $\gamma(\mathbf{e})$, and the microcanonical inverse temperature, $\bar{\beta}(\mathbf{e})$, for the 147-LJ cluster. The inset provides a broader view of the curve.

2. Parametric microcanonical inflection point and Fisher's zeros analysis for $N = 55$ and $N = 147$, inside a sphere of radius $r_c = 3.5\sigma$

Fig. 5 depicts the scaling behavior of $\gamma(\bar{\beta})$ with system size. The data for $L = 55$ particles confined within

a spherical volume of radius $r_c = 3.5\sigma$ are represented by black circles. The knot position corresponds to the transition temperature, $\bar{T}_{knot} = 0.2982(2)$, as indicated by the solid red line. For comparison, the transition temperature associated with dominant zeros is shown by the dashed magenta line. Results for $N = 147$ particles are displayed as red squares for $r_c = 3.5\sigma$ and green diamonds for $r_c = 4.0\sigma$.

A clear shrinkage of the loop towards $\gamma = 0$ is observed with increasing system size, consistent with the expectation from eq. (24). Notably, the loop is slightly smaller for $L = 147$ at $r_c = 4.0\sigma$ compared to $r_c = 3.5\sigma$, as evident in the inset of the figure. It is well-established that for simple systems, the first-order transition line tends towards a critical point with increasing pressure and, consequently, a decrease in latent heat. Based on these considerations, we hypothesize a correlation between the loop size and the inverse of the latent heat, thus, with the distance between dominant zeros. However, a more comprehensive dataset is required to establish a precise mathematical relationship for this dependence.

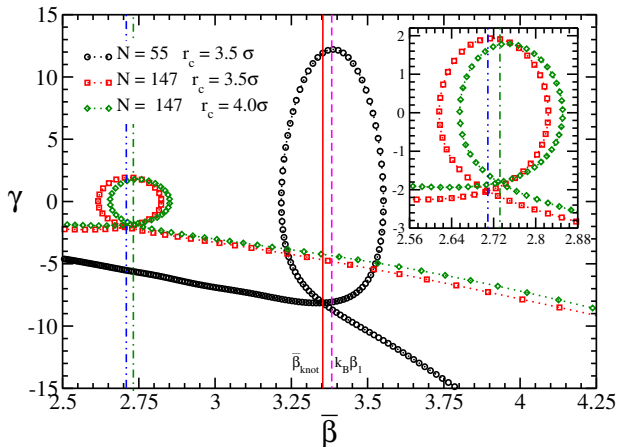


FIG. 5. (Color online) Illustration of the scale behavior of γ described by eq. (24). The inset shows a zoom in the loop of the results for $N = 147$ particles.

Fig. 6 presents the Fisher's zeros map for the Lennard-Jones (LJ) cluster constrained to a sphere of radius $r_c = 3.5\sigma$. We use MPSolve [35, 36] as the root finder. A characteristic pattern of equally spaced vertical lines of zeros is observed, converging towards the real temperature axis, indicative of a first-order phase transition. Panel (a) displays the map for $N = 55$ particles, where the real part of the leading zero corresponds to a transition temperature of $k_B T_1 = 0.2956(4)$ and latent heat of $\mathcal{L} = 30.80(3)$. Panel (b) shows the map for $N = 147$ particles, with a measured transition temperature of $k_B T_1 = 0,3676(4)$ and latent heat of $\mathcal{L} = 51.51(3)$. The zeros map for a 147-particle LJ cluster confined within a sphere of radius $r_c = 4.0\sigma$ can be found in reference [17]. Each symbol in the figure represents a map obtained from an independent simulation, it can be noted that, as it is well-known, the zeros of the partition function are highly sensitive to

statistical fluctuations, except for the dominant zeros.

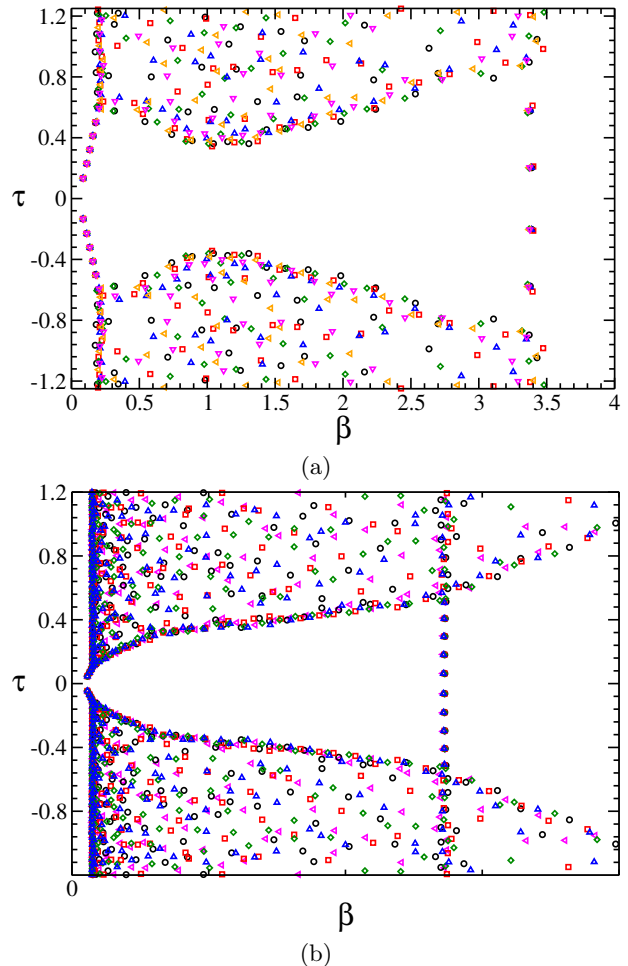


FIG. 6. (Color online) Fisher's zeros map for the LJ cluster constrained to a sphere of radius $r_c = 3.5\sigma$. In panel (a) for $N = 55$ particles and in panel (b) for $N = 147$ particles (see Ref [17] for 147-LJ cluster in $r_c = 4.0\sigma$). Each symbol corresponds to a map obtained from an independent simulation.

The limit of the latent heat to zero toward the critical point, where the entropy becomes continuous, implies that the distance between dominant zeros diverges at the critical point, see eq. (17). Based on these observations, although the densities of zeros have been successfully used to characterize phase transitions [37], we hypothesize that a second-order phase transition can be uniquely characterized by the behavior of its single leading zero complex conjugated pair closest to the real positive axis. This claim is further supported by previous findings where second-order phase transitions were associated with leading zeros that do not exhibit any discernible connected pattern [33, 38]. In the next section, we propose a test of this hypothesis.

B. 2D Ising Model

The two-dimensional (2D) Lenz-Ising model serves as a theoretical framework for the second-order phase transitions [39]. This model considers spin-1/2 particles, arranged in a fixed lattice, that interacts with their nearest neighbors. Lars Onsager derived the exact solution for the square lattice in 1944 [40], where the critical temperature is deduced to be $T_c = 2/\ln(1 + \sqrt{2})$.

For the case where the external magnetic field is zero, the Hamiltonian describing the model is given by

$$\mathcal{H} = -J \sum_{\langle i,j \rangle} \sigma_i \sigma_j, \quad (26)$$

where J is the exchange integral (positive for ferromagnetic and negative for antiferromagnetic interactions), and $\sigma_i = \pm|\sigma|$ represents the spin at site i . Throughout this section, energy is expressed in units $J|\sigma|^2$ and the canonical temperature in units of $J|\sigma|^2/k_B$. We consider a $L \times L$ square lattice with periodic boundary conditions, where L is the linear lattice size. The notation $\langle i,j \rangle$ indicates summation over nearest-neighbor pairs.

1. Parametric microcanonical inflection point analysis for the 2D Ising Model

Recent studies employing conventional microcanonical inflection point analysis of this model [27, 41–43] have reported evidence of higher-order phase transitions in addition to the well-known second-order ferromagnetic/paramagnetic transition. Specifically, two additional transitions were identified: a dependent transition occurring above the critical temperature and an independent transition occurring below it, as illustrated in the next paragraph.

Fig. 7 presents the results of a parametric microcanonical inflection point analysis conducted on the two-dimensional Ising model. The entropy was calculated using the exact solution provided by Beale [44]. Panel (a) illustrates the scaling behavior of the system through results obtained for lattice sizes $L = 32$ (black circles), $L = 64$ (red squares), and $L = 96$ (green diamonds). The exact inverse transition temperature for this model is indicated by the red solid vertical line. Panel (b) details results for $L = 96$. Specifically, this panel displays $\gamma(\bar{\beta})$ (black circles), with the vertical dashed green line marking its peak, which corresponds to a pseudo-second-order phase transition at $\bar{\beta}_{tr(L=96)} = 0.43863$. Additionally, $\delta(\bar{\beta})$ (red squares) is shown. A pseudo-third-order phase transition at $\bar{\beta}_{tr(L=96)} = 0.44673873$ is indicated by the blue dotted-dashed line, which marks the position of a local minimum of $\delta(\bar{\beta})$ with a positive value. A dependent pseudo-third-order transition at $\bar{\beta}_{tr(L=96)} = 0.43515905$ is identified by the magenta double-dotted-dashed line, corresponding to a local minimum of $\delta(\bar{\beta})$ with a negative value. Consistent with prior research [27], which has

demonstrated the evolution of an independent pseudo-fourth-order transition in small systems to a third-order transition with increasing system size (L), this behavior was also observed in the present analysis. The absence of the third-order transition for smaller L is evident in Fig 9 (b), as no positive-valued local minimum in $\delta(\bar{\beta})$ is observed for the exact DOS at $L = 20$.

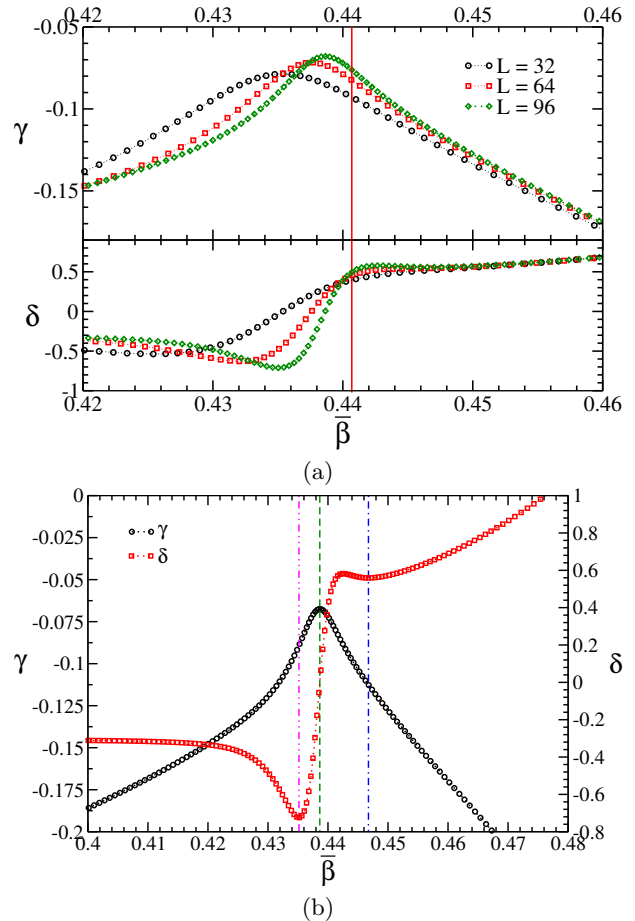


FIG. 7. (Color online) $\gamma(\bar{\beta})$ and $\delta(\bar{\beta})$ for the 2D Ising model. Panel (a) depicts the scaling behavior. Panel (b) shows in details the result for $L = 96$.

2. Fisher leading zero critical behavior analysis

Fig. 8 depicts the Fisher's zeros map for the Ising model on the complex \mathcal{B} -plane, an alternative representation to the conventional x -complex plane [45] or analogous quantities such as $w = 2 \sinh(2\beta)$ [46]. Notably, circles in the x -complex plane are mapped onto vertical lines in the \mathcal{B} -plane. Furthermore, circles with radii exceeding unity correspond to negative temperatures ($\beta < 0$), which are not displayed in our graphs. For this model, negative temperatures mean antiferromagnetic ground states, as the temperature is measured in units of $J|\sigma|^2/k_B$. Owing to the symmetry of the

density of states (DOS) for the Ising model, the magnitudes of the transition temperatures are identical. In Fig. 8, the real part of the leading zero is determined to be $k_B\beta_1 \approx 0.43868$. While exhibiting a vertical line pattern, this map deviates from the characteristic pattern observed in first-order transitions due to the non-uniform spacing of the dominant zeros [47, 48]. Considering system sizes up to $L = 128$, the Finite-size scaling (FSS) analysis of the leading zeros yields an estimate for the critical temperature with an error of approximately 0.02% compared to the exact value. Moreover, this FSS analysis provides an estimate for the critical exponent ν , as shown in Eq. (9), with a 0.7% error relative to the expected value of $\nu = 1$ for the Ising universality class, thereby corroborating the reliability of the analysis.

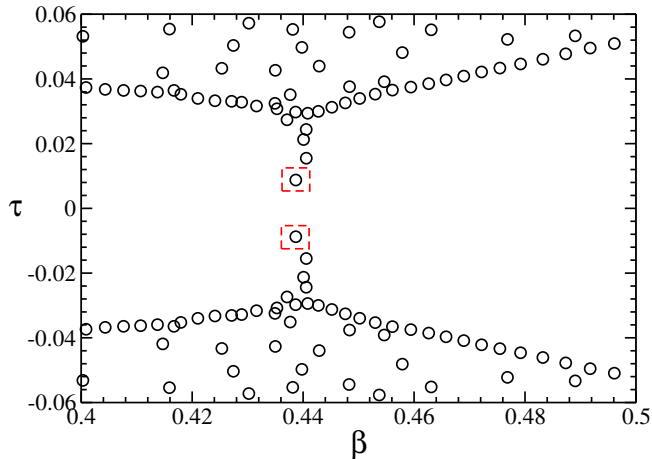


FIG. 8. (Color online) Fisher's Zeros map for the Ising model with linear system size $L = 96$. The red dashed squares indicate the leading zeros.

To test the hypothesis that a single complex-conjugated pair of zeros contains all information of the second-order transition, we excluded the leading zeros from the Fisher zeros map and recomputed the density of states, $\Omega(E)$, by multiplying the remaining binomials as per eq. (8). Subsequently, we performed a parametric microcanonical inflection point analysis to investigate the phase transitions associated with this modified density of states, as depicted in Fig. 9. In panel (a) we observe a flattening of the peak in $\gamma(\bar{\beta})$ when the leading zero complex conjugated pair is excluded. While there is still a local maximum, this feature alone does not definitively indicate a true critical point unless accompanied by clear FSS behavior as dictated by eq. (24). Notably, in the next section, we present an example of non-scaling local maxima in γ .

Due to the inherent error propagation in floating-point multiplication, using 16 bytes floating-point data type, we were able to accurately reproduce the exact DOS from the entire zeros map only for system sizes up to $L = 22$ within the context of validation of our code. For $L = 24$ our computations resulted in an error of up to 10% in the

entropy, whereas for $L = 22$ the error in $S(E)$ was on the order of 10^{-7} . Associated with the well-known deviations from the simple scaling form for small system sizes [49], this limitation precluded a reliable FSS analysis of the modified density of states. It is important to note that, as mentioned before, the absence of a dependent transition does not preclude the existence of an independent transition of a lower order, as the latter serves as a necessary condition for the former, but not vice versa [27]. While it appears that the leading zero alone may encapsulate all the information concerning the critical behavior, since its absence seems to lead to the exclusion of the scaling behavior and also the dependent and independent transitions of higher order close to the critical point, a formal proof of this assertion remains elusive. Therefore, a more systematic investigation is necessary to rigorously establish this claim.

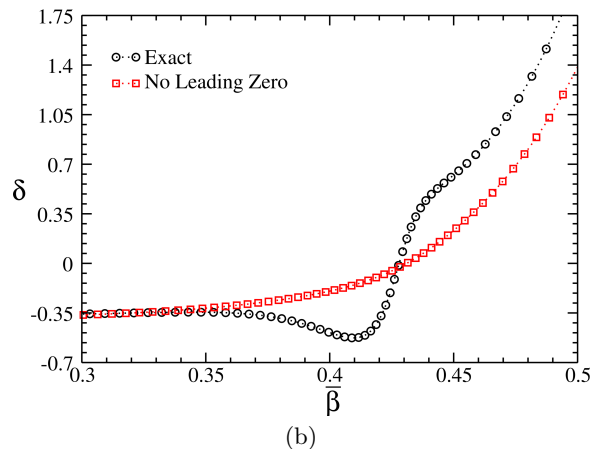
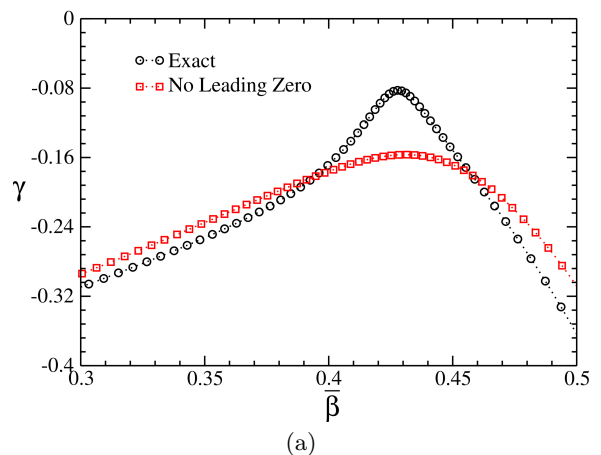


FIG. 9. (Color online) (a) $\gamma(\bar{\beta})$, and (b) $\delta(\bar{\beta})$ for the Ising model with system linear size $L = 20$. Black circles represent the result obtained from the exact DOS and red squares are the results obtained from DOS reconstructed with the absence of the leading zeros complex conjugated pair.

C. XY Model

The Berezinskii-Kosterlitz-Thouless (BKT) transition, exemplified by the XY model, is a topological phase transition driven by the unbinding of vortices at the temperature T_{BKT} . It is characterized by the absence of discontinuities or divergences in any finite-order derivative of the free energy. The XY model describes two-dimensional systems, a prototype being a lattice of spins with continuous symmetry. The state of each spin is characterized by an angular variable, θ_i , denoting its orientation with respect to a fixed reference axis within the plane. Interactions are confined to nearest neighbors, and the Hamiltonian of the system assumes the following form:

$$\mathcal{H} = -J \sum_{\langle i,j \rangle} \cos(\theta_i - \theta_j). \quad (27)$$

In previous work, we investigated this model on a square lattice of dimension $L \times L$ employing Fisher's zeros methodology [50–52]. An example of these mappings on \mathcal{B} plane, instead of the originally complex- x map, is depicted in Fig. 10. Despite the absence of dominant zeros, the BKT transition was identified by examining the internal border of zeros through FSS analysis, where the BKT transition temperature was estimated to be $T_{BKT} = 0.704(3)$. Our findings were in complete concordance with theoretical predictions, enabling the classification of the phase transition as belonging to the BKT universality class.

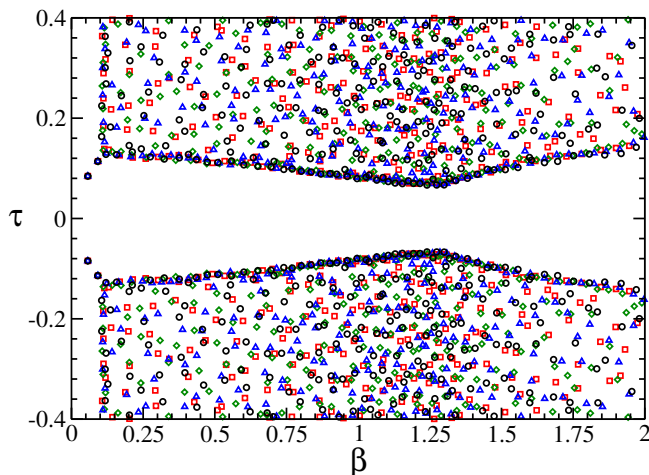


FIG. 10. (Color online) Fisher's Zeros map for the XY model with linear system size $L = 50$. Each symbol corresponds to a map obtained from an independent simulation.

In Fig. 11, we present the parametric microcanonical inflection point analysis for this model. Given that finite-order derivatives of the free energy remain finite and continuous, one can anticipate no indication of a transition in these graphs. Panel (a) of the figure displays $\gamma(\beta)$, where a local maximum with a negative value is observed. However, this feature does not exhibit any discernible scaling

behavior, precluding the identification of a critical point, as expected. This result holds significant importance as it provides evidence that can be used in support of the hypothesis that the leading zero of the partition function encapsulates all critical behavior information, as previously asserted. Panel (b) illustrates $\delta(\beta)$ which similarly shows no evidence of a higher-order transition. Higher-order derivatives are not displayed due to the substantial error caused by the sensitivity of numerical derivatives to statistical fluctuations.

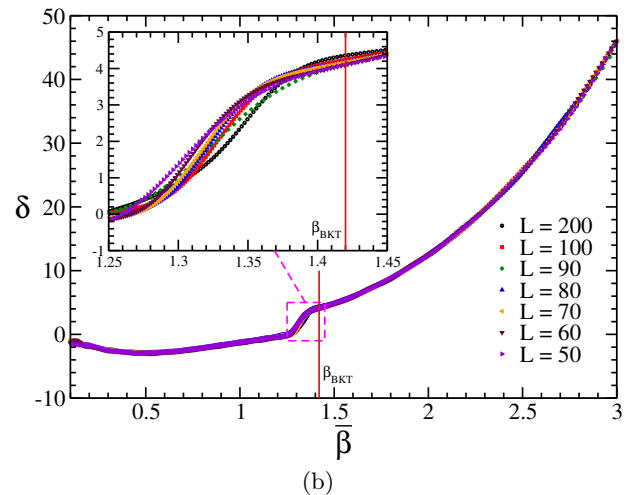
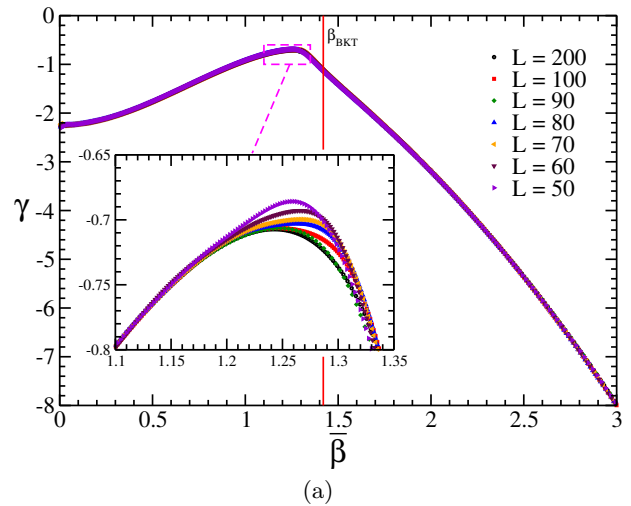


FIG. 11. (Color online) The parametric microcanonical inflection point analysis for the XY-Model. In panel (a) we show $\gamma(\beta)$ and in panel (b) $\delta(\beta)$, for linear system size $L = 50, 60, 70, 80, 90, 100$, and 200 . The vertical red solid line indicates the inverse temperature at the BKT transition for the XY model estimated from the zeros map.

D. Zeeman Model

We chose to study the Zeeman Model as an instance of a system that does not exhibit a phase transition at

any finite temperature. This model consists of N non-interacting $1/2$ -spins particles in a magnetic field, \vec{B} . The Hamiltonian can be expressed as

$$\mathcal{H} = -\mu_B B \sum_{i=1}^N \sigma_i, \quad (28)$$

where we employ reduced units such that $\mu_B = 1$ represents the Bohr magneton, $|\sigma| = 1$ denotes the spin magnitude, and $\sigma_i = \pm 1$. Furthermore, $B = |\vec{B}|$ signifies the strength of the magnetic field, and the Boltzmann constant is set to $k_B = 1$.

The exact number of states with energy E for this model is well-known, as detailed in reference [53]. It is given by

$$\begin{aligned} \Omega(E, N) &= \binom{N}{n} = \frac{N!}{n!(N-n)!}, \\ &= \frac{N!}{\left[\frac{1}{2}\left(N - \frac{E}{B}\right)\right]! \left[\frac{1}{2}\left(N + \frac{E}{B}\right)\right]!}, \end{aligned} \quad (29)$$

where n represents the number of spins aligned with the magnetic field, and consequently, $(N - n)$ is the number of spins anti-aligned with \vec{B} . By directly evaluating the Hamiltonian, the energy density can be expressed as $e = -Bm = -B(2n/N - 1)$, where $m = M/N$ is the magnetization per spin.

The partition function can be written as [53]:

$$\begin{aligned} Z(\mathcal{B}, N) &= e^{-\mathcal{B}BN} \sum_{n=0}^N \binom{N}{n} \left(e^{2\mathcal{B}B}\right)^n, \\ &= e^{-\mathcal{B}BN} \left(1 + e^{2\mathcal{B}B}\right)^N, \\ &= \left[2 \cosh(\mathcal{B}B)\right]^N. \end{aligned} \quad (30)$$

Thus, by inspecting equation (30), $Z = 0$ if $e^{2\mathcal{B}B} = -1$. Thus, $2\mathcal{B}B = \pm i(2k - 1)\pi$, for $k = 1, 2, \dots$. This leads to $\beta_k = 0$ and

$$\tau_k = \pm \frac{(2k - 1)\pi}{2B}, \quad (32)$$

i.e., the Fisher zeros are evenly distributed along the imaginary inverse temperature axis. This analysis explains the presence of a vertical line pattern of zeros near the imaginary axis on the \mathcal{B} maps (which correspond to a unit circle in the complex- x map), interpreted as a transition at infinite temperature. However, a perfect alignment with $\beta = 0$ is not observed in our results due to the exclusion of positive energy values ($E > 0$) from our simulations.

Furthermore, by considering Stirling's approximation, which states that $\ln y! = y \ln y - y + \mathcal{O}(\ln y)$, the parametric curve for $\bar{\gamma}$ can be deduced to be

$$\bar{\gamma}(\bar{\beta}) \approx - \left[\frac{1}{B} \cosh(\bar{\beta}B) \right]^2. \quad (33)$$

This is a function with a negatively valued maximum at $\bar{\beta} = 0$, also signaling the absence of a transition at finite temperature for this model, then corroborating the proposed methodology. Moreover, this peak approaches zero only as $B \rightarrow \infty$.

By comparing with eq. (31), it can be stated that the analytic continuation of eq. (33) exhibits the same zeros as the partition function. At least in this specific case, the Fisher zeros and the zeros of γ coincide across the entire complex plane. However, for other models, this equivalence certainly holds only for the real positive zero, which arises exclusively in the thermodynamic limit.

IV. CONCLUSIONS

In this study, we introduce a novel technique for analyzing phase transitions, utilizing microcanonical quantities with inverse temperature, $\bar{\beta}$, as a parameter. By examining the behavior of thermodynamic quantities, such as entropy and its derivatives, as functions of $\bar{\beta}$, we observe that each type of transition has its own characteristic behavior. To introduce the method we have studied several models in well known universality class.

For first-order transitions, the parametric entropy curve exhibits a characteristic "Z" shape, allowing for an equal-area Maxwell construction. Concurrently, the parametric curve of the second derivative of entropy (γ) forms a loop, with the knot point indicating the transition temperature. This loop structure effectively captures the behavior associated with the first-order transition.

In contrast, for second-order transitions, the parametric analysis of γ reveals a negative-valued peak, consistent with traditional microcanonical inflection point analysis.

We have applied this framework to several model systems, including the Lennard-Jones cluster, the Ising model, the XY model, and the Zeeman model, demonstrating its effectiveness in characterizing first-order, second-order, and Berezinskii-Kosterlitz-Thouless (BKT) transitions.

Furthermore, we have explored the relationship between Fisher zeros and the parametric microcanonical curves, providing valuable insights into the underlying thermodynamic behavior. The proposed method offers a powerful tool for understanding and classifying phase transitions in diverse physical systems.

While the parametric microcanonical inflection point analysis outperforms the Fisher's zeros map analysis in detecting third- and fourth-order transitions, as these appear to be captured primarily by the leading zero that indicates just the second-order transition, the BKT transition seems to be nonconclusive through the former approach even though it is discernible via the latter.

ACKNOWLEDGMENTS

This work received public financial support from Conselho Nacional de Desenvolvimento Científico e Tecnológico (CNPq), Brazil, under grant 409719/2023-4.

AUTHOR DECLARATIONS

The authors have no competing interests to declare that are relevant to the content of this article.

-
- [1] S.A. Kivelson, J.M. Jiang, and J. Chang. *Statistical Mechanics of Phases and Phase Transitions*. Princeton University Press, 2024.
- [2] Brent Fultz. *Phase Transitions in Materials*. Cambridge University Press, 2020.
- [3] Tormod Riste and David Sherrington. *Phase transitions in soft condensed matter*, volume 211. Springer Science & Business Media, 2012.
- [4] A D Linde. Phase transitions in gauge theories and cosmology. *Reports on Progress in Physics*, 42(3):389, mar 1979.
- [5] Tilman Sauer. Statistical theory of equations of state and phase transitions. ii. lattice gas and ising model. *The European Physical Journal Special Topics*, 226(4):539–549, 2017.
- [6] Gregg Jaeger. The ehrenfest classification of phase transitions: Introduction and evolution. *Arch. Hist. Exact Sci.*, 53(1):51–81, May 1998.
- [7] John Michael Kosterlitz. Nobel lecture: Topological defects and phase transitions. *Rev. Mod. Phys.*, 89:040501, Oct 2017.
- [8] M. Planck. Phase transitions and the distribution of temperature zeros of the partition function. *Annalen der Physik*, 4:553–562, 1901.
- [9] Herbert B Callen. *Thermodynamics and an introduction to thermostatistics; 2nd ed.* Wiley, New York, NY, 1985.
- [10] D.H.E. Gross. *Microcanonical Thermodynamics: Phase Transitions in "small" Systems*, chapter 2. World Scientific lecture notes in physics. World Scientific, 2001.
- [11] Dieter H.E. Gross. A new thermodynamics from nuclei to stars. *Entropy*, 6(1):158–179, 2004.
- [12] J.H. Luscombe. *Statistical Mechanics: From Thermodynamics to the Renormalization Group*, chapter 4, pages 86–87. CRC Press, 2021.
- [13] J. C. S. Rocha, R. F. I. Gomes, W. A. T. Nogueira, and R. A. Dias. Estimating the number of states of a quantum system via the rodeo algorithm for quantum computation. *Quantum Information Processing*, 23(10):345, Oct 2024.
- [14] T. D. Lee and C. N. Yang. Statistical theory of equations of state and phase transitions. ii. lattice gas and ising model. *Phys. Rev.*, 87:410–419, Aug 1952.
- [15] M.E. Fisher. The nature of critical points. In W. E. Brittin, editor, *Lectures in Theoretical Physics, Volume VII C - Statistical Physics, Weak Interactions, Field Theory, Lectures Delivered at the Summer Institute for Theoretical Physics*. University of Colorado Press, Boulder, 1965.
- [16] Juan Carrasquilla and Roger G. Melko. Machine learning phases of matter. *Nature Physics*, 13(5):431–434, May 2017.
- [17] J C S Rocha and B V Costa. Connecting the unstable region of the entropy to the pattern of the fisher zeros map. *Journal of Statistical Mechanics: Theory and Experiment*, 2024(3):033201, feb 2024.
- [18] C. Itzykson, R.B. Pearson, and J.B. Zuber. Distribution of zeros in ising and gauge models. *Nuclear Physics B*, 220(4):415–433, 1983.
- [19] Michael Bachmann. *Thermodynamics and statistical mechanics of macromolecular systems*, chapter 2, pages 62–65. Cambridge University Press, Cambridge, 2014.
- [20] Mark P. Taylor, Pyie Phyo Aung, and Wolfgang Paul. Partition function zeros and phase transitions for a square-well polymer chain. *Phys. Rev. E*, 88:012604, Jul 2013.
- [21] B. V. Costa, L. A. S. Mól, and J. C. S. Rocha. Energy probability distribution zeros: A route to study phase transitions. *Computer Physics Communications*, 216:77–83, 2017.
- [22] B. V. Costa, L. A. S. Mól, and J. C. S. Rocha. The zeros of the energy probability distribution - a new way to study phase transitions -. *Journal of Physics: Conference Series*, 921(1):012004, nov 2017.
- [23] J. J. Carvalho and A. L. Mota. Finding the dominant zero of the energy probability distribution. *International Journal of Modern Physics C*, 32(12):2150155, 2021.
- [24] R. G. M. Rodrigues, B. V. Costa, and L. A. S. Mól. Moment-generating function zeros in the study of phase transitions. *Phys. Rev. E*, 104:064103, Dec 2021.
- [25] P. M. Stevenson. Optimized perturbation theory. *Phys. Rev. D*, 23:2916–2944, Jun 1981.
- [26] P.M. Stevenson. Resolution of the renormalisation-scheme ambiguity in perturbative qcd. *Physics Letters B*, 100(1):61–64, 1981.
- [27] Kai Qi and Michael Bachmann. Classification of phase transitions by microcanonical inflection-point analysis. *Phys. Rev. Lett.*, 120:180601, Apr 2018.
- [28] Stefan Schnabel, Daniel T. Seaton, David P. Landau, and Michael Bachmann. Microcanonical entropy inflection points: Key to systematic understanding of transitions in finite systems. *Phys. Rev. E*, 84:011127, Jul 2011.
- [29] Thomas Vogel, Ying Wai Li, Thomas Wüst, and David P. Landau. Generic, hierarchical framework for massively parallel wang-landau sampling. *Phys. Rev. Lett.*, 110:210603, May 2013.
- [30] Alexandra Valentim, Julio C S Rocha, Shan-Ho Tsai, Ying Wai Li, Markus Eisenbach, Carlos E Fiore, and David P Landau. Exploring replica-exchange wang-landau sampling in higher-dimensional parameter space. *Journal of Physics: Conference Series*, 640(1):012006, sep 2015.
- [31] B.B. Rodrigues, J.C.S. Rocha, and B.V. Costa. Phase diagram of flexible polymers with quenched disordered charged monomers. *Physica A: Statistical Mechanics and its Applications*, 604:127787, 2022.
- [32] Pavel A. Frantsuzov and Vladimir A. Mandelshtam. Size-temperature phase diagram for small lennard-jones clusters. *Phys. Rev. E*, 72:037102, Sep 2005.

- [33] Julio C.S. Rocha, Stefan Schnabel, David P. Landau, and Michael Bachmann. Leading fisher partition function zeros as indicators of structural transitions in macromolecules. *Physics Procedia*, 57:94–98, 2014. Proceedings of the 27th Workshop on Computer Simulation Studies in Condensed Matter Physics (CSP2014).
- [34] Pierre Labastie and Robert L. Whetten. Statistical thermodynamics of the cluster solid-liquid transition. *Phys. Rev. Lett.*, 65:1567–1570, Sep 1990.
- [35] Dario Andrea Bini and Giuseppe Fiorentino. Design, analysis, and implementation of a multiprecision polynomial rootfinder. *Numerical Algorithms*, 23(2):127–173, 2000.
- [36] Dario A. Bini and Leonardo Robol. Solving secular and polynomial equations: A multiprecision algorithm. *Journal of Computational and Applied Mathematics*, 272:276–292, 2014.
- [37] W. Janke and R. Kenna. The strength of first and second order phase transitions from partition function zeroes. *Journal of Statistical Physics*, 102(5):1211–1227, Mar 2001.
- [38] Julio C. S. Rocha, Stefan Schnabel, David P. Landau, and Michael Bachmann. Identifying transitions in finite systems by means of partition function zeros and microcanonical inflection-point analysis: A comparison for elastic flexible polymers. *Phys. Rev. E*, 90:022601, Aug 2014.
- [39] Stephen G. Brush. History of the lenz-ising model. *Rev. Mod. Phys.*, 39:883–893, Oct 1967.
- [40] Lars Onsager. Crystal statistics. i. a two-dimensional model with an order-disorder transition. *Phys. Rev.*, 65:117–149, Feb 1944.
- [41] Kedkanok Sitarachu and Michael Bachmann. Phase transitions in the two-dimensional ising model from the microcanonical perspective. *Journal of Physics: Conference Series*, 1483(1):012009, feb 2020.
- [42] K Sitarachu, R K P Zia, and M Bachmann. Exact microcanonical statistical analysis of transition behavior in ising chains and strips. *Journal of Statistical Mechanics: Theory and Experiment*, 2020(7):073204, jul 2020.
- [43] Kedkanok Sitarachu and Michael Bachmann. Evidence for additional third-order transitions in the two-dimensional ising model. *Phys. Rev. E*, 106:014134, Jul 2022.
- [44] Paul D. Beale. Exact distribution of energies in the two-dimensional ising model. *Phys. Rev. Lett.*, 76:78–81, Jan 1996.
- [45] Nelson A. Alves, J. R. Drugowich de Felicio, and Ulrich H. E. Hansmann. A new look at the 2d ising model from exact partition function zeros for large lattice sizes. *International Journal of Modern Physics C*, 08(05):1063–1071, 1997.
- [46] W. Janke, D.A. Johnston, and R. Kenna. Phase transition strength through densities of general distributions of zeroes. *Nuclear Physics B*, 682(3):618–634, 2004.
- [47] Peter Borrmann, Oliver Mülken, and Jens Harting. Classification of phase transitions in small systems. *Phys. Rev. Lett.*, 84:3511–3514, Apr 2000.
- [48] Nelson A. Alves, Jeaneti P. N. Ferrite, and Ulrich H. E. Hansmann. Numerical comparison of two approaches for the study of phase transitions in small systems. *Phys. Rev. E*, 65:036110, Feb 2002.
- [49] D. P. Landau. Finite-size behavior of the ising square lattice. *Phys. Rev. B*, 13:2997–3011, Apr 1976.
- [50] J. C. S. Rocha, L. A. S. Mól, and B. V. Costa. Using zeros of the canonical partition function map to detect signatures of a berezinskii–kosterlitz–thouless transition. *Computer Physics Communications*, 209:88–91, 2016.
- [51] T.P. Figueiredo, J.C.S. Rocha, and B.V. Costa. Topological phase transition in the two-dimensional anisotropic heisenberg model: A study using the replica exchange wang–landau sampling. *Physica A: Statistical Mechanics and its Applications*, 488:121–131, 2017.
- [52] B. V. Costa, L. A. S. Mól, and J. C. S. Rocha. A new algorithm to study the critical behavior of topological phase transitions. *Brazilian Journal of Physics*, 49(2):271–276, Apr 2019.
- [53] S. Salinas. *Introduction to Statistical Physics*. Graduate Texts in Contemporary Physics. Springer New York, 2001.